Reply to Reviewer #2

We thank you for your time and efforts in reviewing our manuscript. We considered all comments and suggestions and provided our detailed point-by-point responses below.

General Comments:

This study examined the influences of the inner eyewall structure on the moat development, spiral rainband and subsequent secondary eyewall using a pair of model simulations with only differing horizontal grid spacing. While I believe the manuscript provides a nice discussion on the role of the strength of the inner eyewall in modifying the diabatic cooling and upper-level inflow radially outward of the primary eyewall and beneath the anvil, I believe the analysis fails to connect this cooling to the boundary layer processes which are likely forcing the secondary eyewall formation. I also have specific concerns on the choice of comparing only two simulations with differing horizontal gird spacing, specifically the fact that the CTL simulation questionably uses a PBL parameterization in the 'gray zone' (0.3 km) and NSEF uses horizontal grid spacing of 1 km and a PBL parameterization.

Reply: Thank you very much for your comments.

We added more discussions in the revised manuscript to consider the boundary layer processes on the SEF (please see our detailed responses to specific comments 1 and 2). We also conducted more simulations using the LES by turning off the PBL parameterization with the grid spacing of 0.3 km. Related discussions are also provided below with a response to the specific comment 3.

Specific Comments:

1. The choice of comparing two simulations with different innermost grid spacing (0.3 km vs 1 km) is odd to me. For one, grid spacing of 0.3 km is within the turbulent 'gray zone' so the choice of using a PBL parameterization is questionable (e.g., Green and Zhang 2015 and Honnert et al. 2020). In addition, the finest resolved eddies will be different between the two simulations, and it is not clear to me how to interpret these differences in terms of the results presented. This is especially true

in comparing with the results of Green and Zhang (2015). Green and Zhang showed that the development of the secondary eyewall in their simulations (ranging in horizontal grid spacing from 111 m – 3 km) was sensitive to how the turbulence was parameterized. More specifically, they noted that none of the simulations without a planetary boundary layer parametrization simulated the development of a secondary eyewall, suggesting strong sensitivity of secondary eyewall formation to the parameterization of turbulence in the 'gray zone'. I think it is important that the authors reconsider their choice in comparing two simulations with different horizontal grid spacing in order to more easily interpret their results.

Reply:

With and without a PBL scheme at 333-m resolution: A 333-m resolution is in the gray zone. Following Green and Zhang (2015), *we conducted a sensitivity using the large-eddy simulation (LES)* for the 333-m domain by turning off the PBL scheme and replacing it with a new SGS parameterization scheme, i.e., the nonlinear backscatter with anisotropy (NBA) scheme (Mirocha et al. 2010). In addition, we also conducted another experiment using LES with a decreasing horizontal resolution of 111 m (1801*1801 grid points). Both the two LES experiments are initialized at the same time as that used in CTL and NSEF. The corresponding horizontal resolutions are 27 km, 9 km, 3 km, 1 km, 1/3 km (~ 333 m), and 1/9 km (~ 111 m). The lateral boundary conditions for the nested domains are provided by their parent domain.

Figure R2.1 shows the horizontal distribution of the radar reflectivity from the LES experiment with 333-m and 111-m grid spacing. Although the inner-core structure and intensity change are influenced by the finest resolved eddies, the SEF occurs in the two LES experiments at different times. Why SEF occurs without using a PBL scheme in our simulations but not in those by Green and Zhang (2015) is out of the scope of this study. Green and Zhang (2015) proposed that no SEF with the LES via the NBA scheme due to the significant impacts on the PBL structure and thus the evolution of TCs. Our results suggest *the SEF might not be so strong sensitive to the parameterization of turbulence in the 'gray zone'*. However, the

PBL processes will affect the inner-core structures that are important to the SEF as stated in our manuscript. The effect of the PBL processes and eddies on the eyewall structures of TC is needed more testing and discussion.

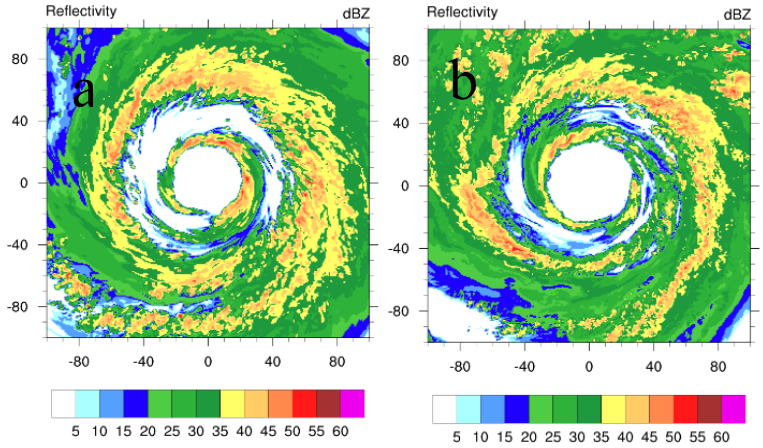

Figure. R2.1 Horizontal distributions of the radar reflectivity at 5-km height (a) at 42 h for the LES with 333-m grid spacing and (b) 36 h for LES with 111-m grid spacing.

Model grid spacing: Increasing horizontal spacing of models presents promising results in the reproduction of the inner-core structures and the intensity changes of TCs. The SEF in our simulations is not sensitive to the parameterization of turbulence in the gray zone (333 m, Fig. R2.1a) except for the timing of the SEF. The main objective of our study is to examine the impacts of changing inner-core structures on the formation of the moat and the secondary eyewall. *We think any method that can affect the structure and intensity of TCs can be used, such as changing the horizontal and vertical resolutions and using different PBL schemes.* Therefore, we compare two simulations with different horizontal grid spacing in order to examine the roles of the inner eyewall structure in the formation of the moat and the secondary eyewall. The effect of the PBL processes and eddies on the changes of the eyewall structures with different grid spacings is unclear and needed more examination. We choose two simulations with and without the SEF to conduct our study in order to make our conclusions stronger. In the revision, we try our best to make discussions concise and easy to be understood.

2. Partially related to my first comment, I am not convinced that the differences in

secondary eyewall formation can be completely attributed to the differences in the inner eyewall structure and not other differences related to the varying horizontal grid spacing between the two simulations and small-scale boundary layer perturbations, potentially related to differences in the model representation of turbulence. As one example, Zhang et al. (2014) demonstrated that secondary eyewall formation is sensitive to very small differences in initial conditions. As a result, I recommend the authors consider revisiting the role of the inner eyewall structure in secondary eyewall formation using a small ensemble with the same model set up.

Reply:

For the boundary effects, we examined the convergence within the boundary layer for the two simulations in Fig. R2.2. There is convergence at radii from 80 km to 120 km where the SEF occurs (Fig. R2.2b), while strong divergence occurs in NSEF from 100-km to 170-km radii. A possible answer to the different structures within the PBL between the NSEF and CTL is that: the moat subsidence in CTL descends into the boundary layer and its related divergent flow meets with boundary inflows, leading to convergence at radii from 80 km to 120 km where the SEF occurs (Fig. R2.3b). On the other hand, the different resolved eddies related to the varying horizontal grid spacing may also introduce different PBL structures, which is out of the scope of our present manuscript focusing on the influences of the eyewall structure on the SEF.

We *did a set of sensitivity experiments by changing the microphysics schemes with the same grid spacing of 333 m instead of a small ensemble since the computation resources and time are limited*. The microphysics schemes used are WSM6, WDM6, Thompson, and Lin. Figure R2.4 shows that the SEF occurs in simulations with different microphysics schemes. The SEF occurs later in WDM6, Thompson, and Lin than that in WSM6. In WDM6, the inner-eyewall convection does not develop vigorously from 20 h to 30 h. After 30 h, the inner-eyewall convection develops vigorously with strong eyewall updrafts shown in Fig. 2.4f. Thus, the SEF occurs around 48 h, which is 16-h later than that in WSM6. In

Thompson and Lin, although the inner-eyewall updrafts are stronger than that in WSM6, the SEF occurs later than that in WSM6 due to different inner-eyewall structures. Figure R2.4 shows that the inner-eyewall expands from 24 h to 48 h, leading to the large-sized eyewall in Thompson and Lin compared to that in WSM6. Therefore, the SEF occurs earlier in WSM6 than that in Thompson and Lin. The sensitivity tests support our results that the SEF is sensitive to the inner-eyewall structure changes. And the SEF occurs when the eyewall updrafts are stronger, and the inner-eyewall convection becomes more compacted.

Moreover, we think that the effects of grid spacing on turbulence and convection can be reflected, to some extent, by the evolution of the eyewall convection. And the changes of the eyewall structures can be caused by any factor (like the different grid spacings, microphysics schemes, and initial vortex, etc.). The purpose of our study is to investigate the possible effects of the structural changes of the inner eyewall on the formation of the moat and the secondary eyewall, while understanding why eyewall structures differ to different factors is beyond the scope of our current study. Your suggestions have inspired us to do more research to understand how different microphysics schemes work on the SEF and to investigate the reliability of the microphysics schemes on the SEF.

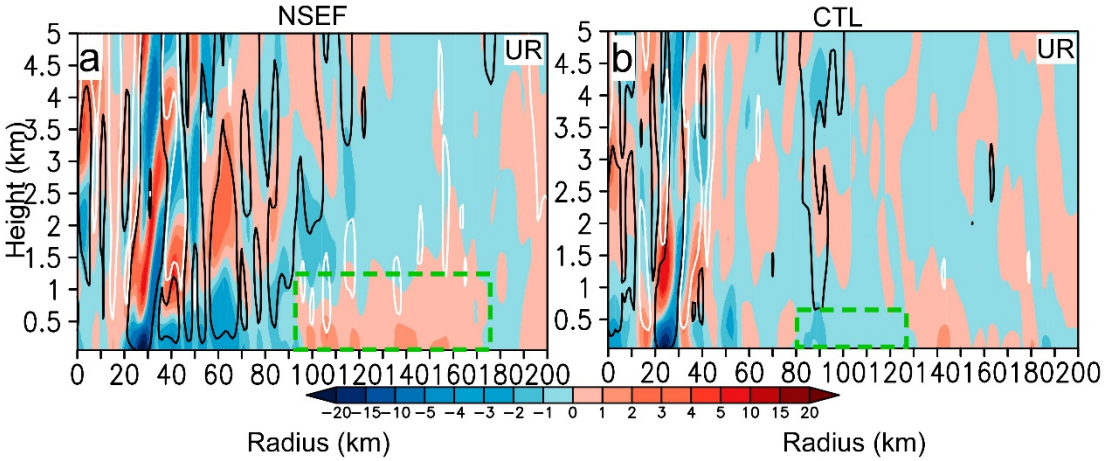

Figure. R2.2 Radius-height cross-sections of the quadrant-mean divergence (shaded, 10^{-4} s^{-1}) superimposed with the vertical wind (black lines of 0.1 m s^{-1} and white lines of -0.1 m s^{-1}) for the (a, b) upshear-right quadrant at 30 h for (a) NSEF and (b) CTL.

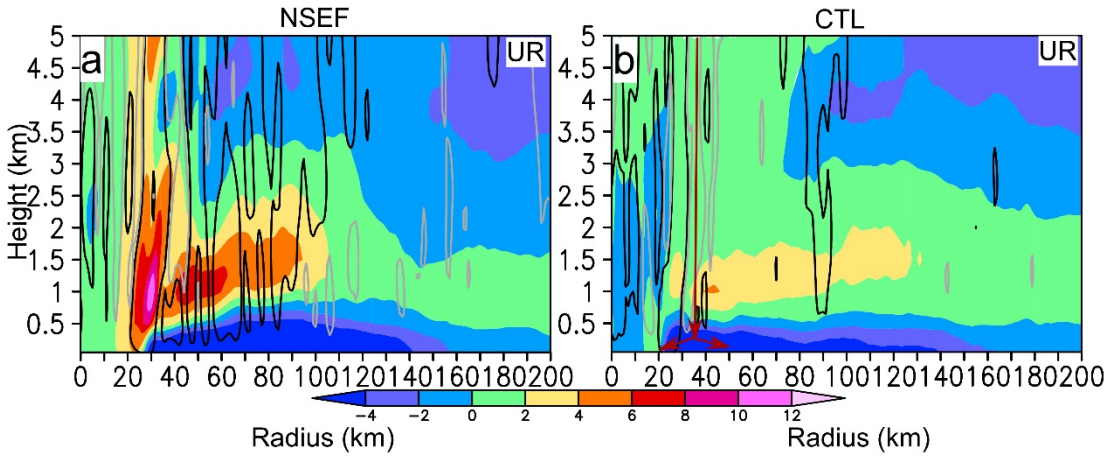

Figure. R2.3 Radius-height cross-sections of the quadrant-mean radial (shaded, m s^{-1}) superimposed with the vertical wind (black lines of 0.1 m s^{-1} and white lines of -0.1 m s^{-1}) for the (a, b) upshear-right quadrant at 30 h for (a) NSEF and (b) CTL. Red arrows indicate the subsidence and divergence.

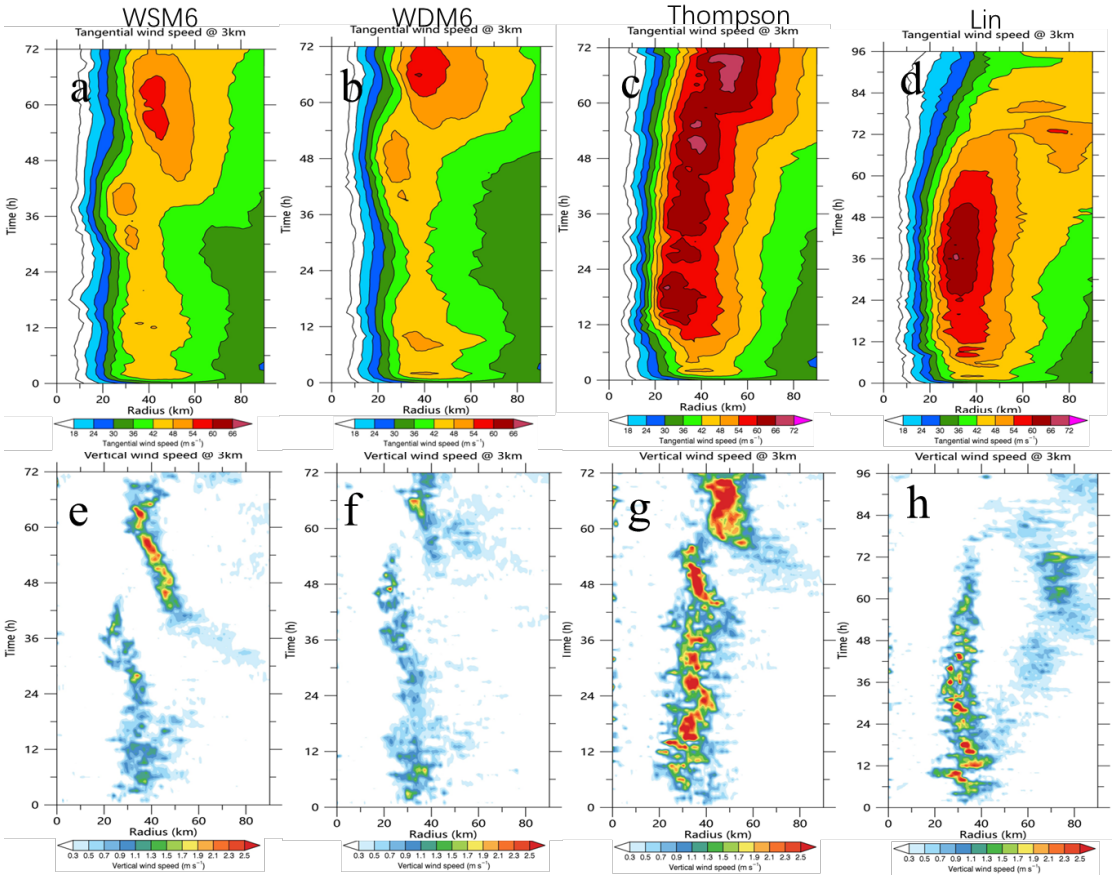

Figure R2.4 Radius-time cross-sections of the azimuthal mean (a-d) tangential wind (m s^{-1}) and (e-h) vertical motion (m s^{-1}) at z = 3 km for (a, e) WSM6, (b, f) WDM6, (c, g) Thompson, and (d, h) Lin.

3. One additional aspect lacking in the current analysis is a connection between the

increased cooling radially outward of the inner eyewall and the mechanisms forcing the secondary eyewall formation. As an example, the authors should try and link this cooling to the boundary layer processes commonly discussed in secondary eyewall formation (e.g., Chen and Wu 2018, Fischer et al. 2020, Wang and Tang 2020) or describe some other relevant process (e.g., Trabing and Bell 2021). It was difficult for me to discern how, or if, the boundary layer forcing changed between these two simulations leading up to secondary eyewall formation and, if so, how that is related to the increased cooling radially outward of the primary eyewall. I suggest the authors take a closer look at any changes in the boundary layer forcing, such as convergence in the vicinity of the secondary eyewall and/or differences in the surface fluxes, and relate these differences back to the inner eyewall structure and the cooling already discussed in the manuscript.

Reply: Thank you for your comments.

In our manuscript, we found, in response to the diabatic warming in the eyewall with strong updrafts and large quantities of hydrometeors, an upper-level dry inflow occurs below the anvil. The drying effects caused by the inflow enhance diabatic cooling below the anvil, which causes negative buoyancy and prompts the subsidence. As feedback, the diabatic cooling further enhances the upper-level inflow. The moat forms with subsidence, which separates the inner eyewall from the outer convection. In this revision, we added more discussions on the SEF related to the changes in the boundary layer forcing. Figures R2.2 and R2.3 show that *the moat subsidence (gray lines in Fig. R2.3b) descends into the boundary layer and its related divergent flow meets with the boundary inflows outside the moat. As a result, convergence occurs at radii from 80 km to 120 km where the SEF occurs in CTL (Figure R2.2b). Moreover, the middle-level moist inflows associated with the outer rainbands travel radially inward and also contribute to the SEF by intensifying the wind field through the inward transport of large angular momentum*. In contrast, there is divergence appearing in NSEF from 100-km to 170-km radii, and strong convergence is located under the broad single eyewall in NSEF.

Following the azimuthal extension of the diabatic cooling under the anvil (Fig.

11 in the revision, here is Fig. R2.5), the subsidence of moat becomes symmetric. Figure R2.6 examines the azimuthal-time cross-sections of the convergence at radii of 80-120 km below 1-km height. *The notable feature for the SEF is the enhanced convergence within the boundary layer along with the azimuthal extension of the moat subsidence. The enhanced convergence forces convection and increases the axisymmetric tangential wind via the axisymmetric dynamical process with the large filamentation time (Terwey and Montgomery 2008)*. Figure R2.6 and their related discussions are added in the revision.

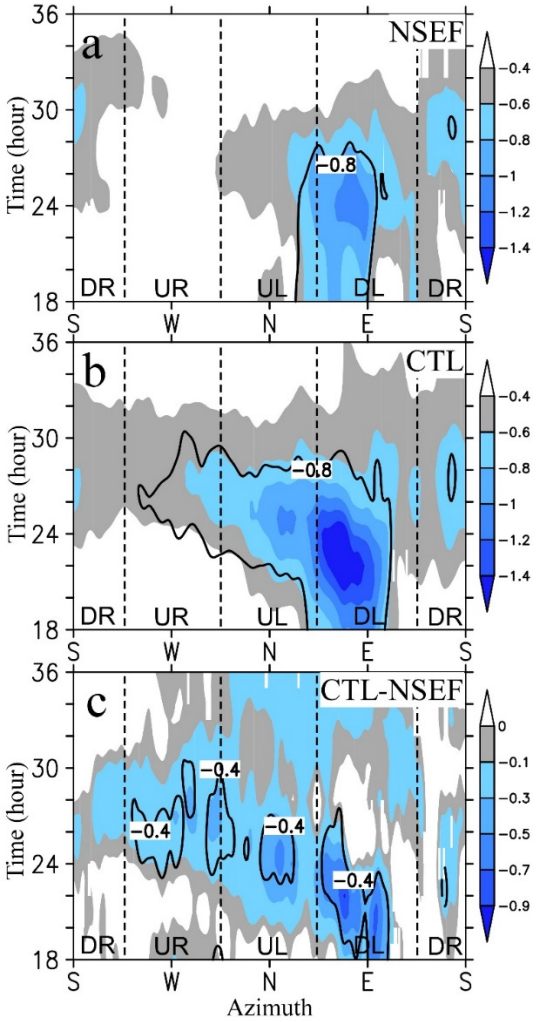

Figure. R2.5 Azimuthal-time cross-sections of the layer-mean (11.5-12.5 km) diabatic cooling (shaded, 10^{-3} K s^{-1}) and subsidence (contour, m s^{-1}) averaged within a radial distance of 25 km starting from the radius of 5-km outside the eyewall (RMW+5 km to RMW+30 km) of (a) NSEF, (b) CTL, and (c) differences between CTL and NSEF. The black contours are -0.8 m s^{-1} in (a, b) and -0.4 m s^{-1} in (c). The black dashed lines indicate the quadrants relative to the large-scale vertical wind shear.

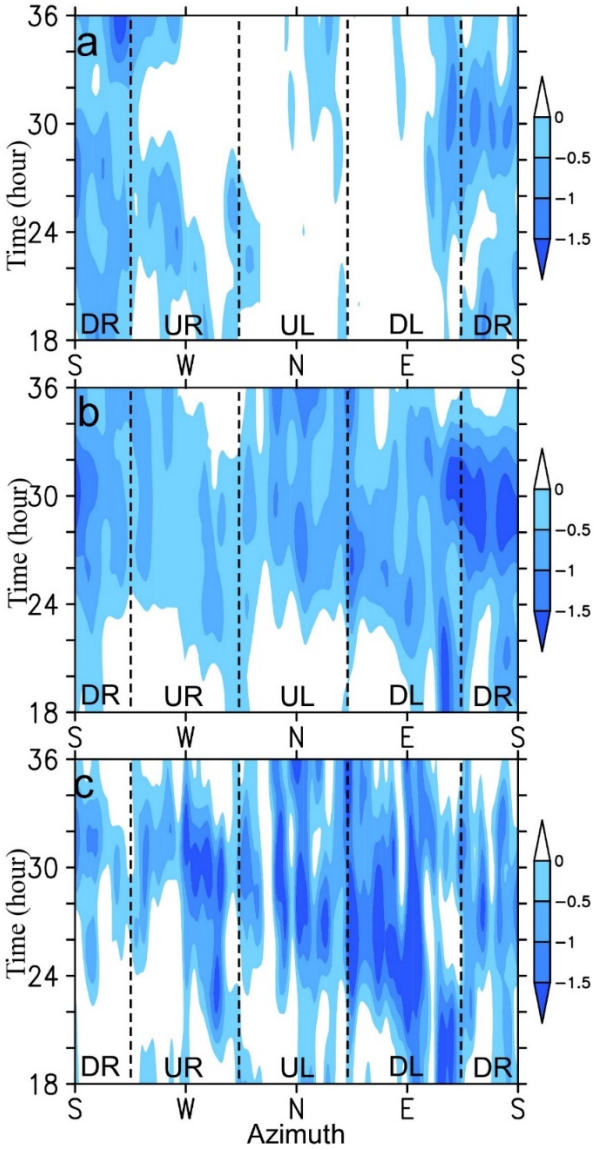

Figure. R2.6 Azimuthal-time cross-sections of the layer-mean (0.05-1.0 km) convergence (shaded, 10^{-4} s^{-1}) averaged from 80-km to 120-km radii of (a) NSEF, (b) CTL, and (c) differences between CTL and NSEF. The black dashed lines indicate the quadrants relative to the large-scale vertical wind shear.

4. I recommend adding column labels for 'CTL' and 'NSEF' on Figures 2–4, similar to that in Figure 8.

   Thanks. Labels are added on the revised Figs. 2-4.

5. (L137–140) Are these fluctuations in Vmax in CTL associated with the azimuthal mean structure (wavenumber-0) or predominantly higher wavenumbers? My speculation is these gusts are likely related to higher wavenumber structures simulated in CTL but please clarify in the manuscript if possible.

Yes, the Vmax shown in Fig. 1 is the maximum 10-m wind, not the azimuthal mean. Those are clarified in the revision as "*There are pronounced fluctuations in the V_{MAX} in CTL, which are related to small-scale or higher wavenumber structures simulated with a finer grid spacing*".

6. I am confused by the buoyancy perturbation analysis discusses (e.g., L209–214 and Eq. 1). How are the wavenumber 0 and 1 components of the perturbation field calculated? Are these related to the full wind field or only the right of shear quadrant? Also, it appears that A^0 is simply a 2d average. I would recommend refining this term as so as not be confused with the wavenumber 0 component.

Thank you for your suggestion. Discussions about the perturbation are revised as follows: *the perturbation associated with the buoyance calculation is defined as* $A'(\lambda,r,z) = A(\lambda,r,z) - A_0(z) - A^0(r,z) - A^1(\lambda,r,z)$, *where A represents any variable in a cylindrical coordinate* (λ,r,z), *λ, r, z are the azimuthal angle, the radius from the TC center, and the vertical height axis, respectively,* $A_0(z)$ *is the 1-km model-domain mean,* $A^0(r,z)$ *and* $A^1(\lambda,r,z)$ *are the wavenumber-0 and -1 components of the field (i.e.,* $A(\lambda,r,z) - A_0(z)$*) for the whole domain, where* $\lambda \in (0{\sim}2\pi)$. *The term of* $A_0(z) + A^0(r,z) + A^1(\lambda,r,z)$ *denotes the reference state for the buoyance analysis*.

7. Why was only the upshear-right quadrant chosen to discuss/show in the manuscript? Please clarify in the manuscript or consider also adding some discussion on other shear-relative quadrants.

Thank you for your suggestion. We have examined and found that all quadrants fit our interpretations. For example, figure R2.7 shows the diabatic heating, the sublimation cooling, and the SEE-diagnosed secondary circulation forced by the diabatic heating and the sublimation cooling for the upshear-left and downshear-right quadrants. The SEE-derived results indicate that the upper-level warming-induced inflows cause the drying effect and promote the sublimation cooling, which is important to force the subsidence and the moat formation.

The above discussions were not added in the revision in case of repeating words. Based on your suggestions, we have added an explanation in section 5.1 as follows to explain why only the upshear-right quadrant is shown in the manuscript: *Quadrant-mean variables relative to the large-scale vertical wind shear are examined to analyze the moat and outer eyewall formation in our following discussions due to the asymmetric structure of TCs. Examinations show that all quadrants present similar results of the buoyancy, the following SEE diagnoses, and their related structures (not shown here). In order to be concise, only one quadrant field (i.e., the upshear-right quadrant) is chosen and discussed in this study.*

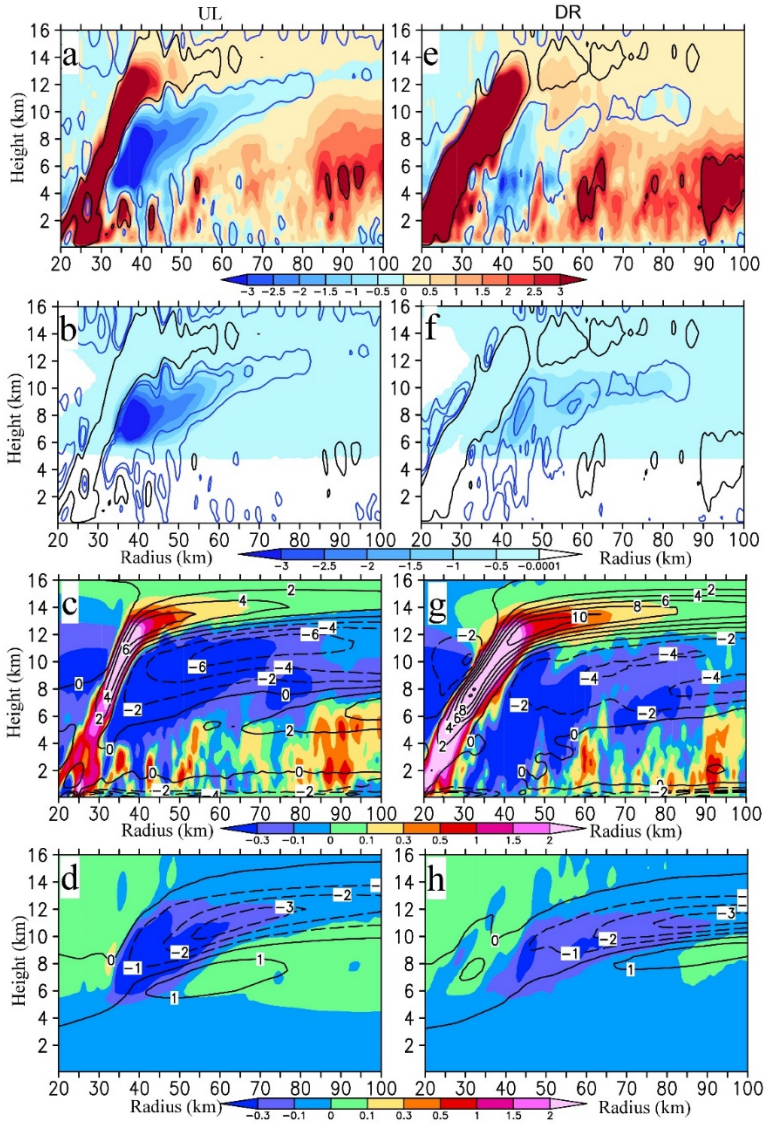

Figure R2.7 Radius-height cross-section of the quadrant-mean (a, e) diabatic heating rate (shaded, 10^{-3} K s^{-1}), (b, f) sublimation cooling rate (shaded, 10^{-3} K s^{-1}), (c, g) vertical (shaded, m s^{-1}) and radial (contours, m s^{-1}) wind forced by the diabatic

heating, and (d, h) vertical and radial wind forced by the sublimation cooling at 30 h of simulation. Left (right) columns are for the upshear-left (downshear-right) quadrant.

8. I strongly recommend changing Figures 11 and 14 to clearly depict/highlight the quadrants in a shear relative coordinate system, as opposed to the cardinal directions currently used.

   Changed as your recommendation.

9. It is not clear how Eq. (2) is being solved. Please clarify in the manuscript.

   It is clarified in section 5.3 as follows: "*In this study, the SEE is solved for the quadrant-mean field using the WRF output at 1-h intervals. The quadrant-mean tangential wind and potential temperature are smoothed by 10 passes of a 1-2-1 smoother before solving the SEE, which can reduce the problematic issues in solving the SEE as done by Zhu and Zhu (2014). The heating forcing term is obtained directly from WRF outputs. The solver of the Multigrid Software For Elliptic Partial Differential Equations (Adams 1989) is used to solve the differential equation. The boundary conditions are set to* $\Psi = 0$ *at r=0 km, z=0 km, and z=18 km and* $\frac{\partial \Psi}{\partial r} = 0$ *at r=110 km*".

Technical Corrections:

1. L22: change "is to further examine" to "further examines"

   Changed.

2. L23: The sentence appears incomplete I suggest adding "in the secondary eyewall formation" after "the role of the inner eyewall structure"

   Added.

3. L46–48: Please be more descriptive here on what you mean by "a consensus has not been reached", in terms of what?

   It is changed to "*a consensus in terms of the intrinsic processes to the SEF has not*

been reached so far."

4. L85–87: This sentence appears incomplete, please revise.

   It is revised to "*Zhu and Zhang (2006) proposed that the timing of the SEF differs as the inner-core structure of the simulated storm changes with varying cloud microphysics processes*".

5. L203: Suggest changing "encircle" to "axisymmetrize".

   Changed.

6. L207–209: This sentence is unclear, please revise.

   This sentence is deleted.

7. L262–263: Change "much diabatic warming" to "more diabatic warming".

   Changed.

8. L346–347: This sentence is unclear, please revise or remove it.

   It has been removed.

References:

Adams, J. (1989), MUDPACK: Multigrid fortran software for the efficient solution of linear elliptic partial differential equations, Appl. Math. Comput., 34, 113–146, doi:10.1016/0096-3003(89)90010-6.

Cheng, C.-J., and C.-C. Wu (2018), The role of WISHE in Secondary Eyewall Formation, J. Atmos. Sci., 11, 3823–3841, doi:10.1175/JAS-D-17-0236.1.

Fischer, M. S., R. F. Rogers, and P. D. Reasor (2020), The rapid intensification and Eyewall Replacement Cycles of Hurricane Irma, Mon. Wea. Rev., 3, 981–1004, doi:10.1175/MWRD-19-0185.1.

Green, B. W., and F. Zhang (2015), Numerical simulations of Hurricane Katrina (2005) in the turbulent gray zone, J. Adv. Model. Earth Syst., 07, doi:10.1002/2014MS000399.

Honnert, R., Efstathiou, G., Beare, R., Ito, J., Lock, A., Neggers, R., et al. (2020). The atmospheric boundary layer and the "gray zone" of turbulence: A critical review. Journal of Geophysical Research: Atmospheres, 125, e2019JD030317. https://doi.org/10.1029/2019JD030317

Mirocha, J. D., J. K. Lundquist, and B. Kosović (2010), Implementation of a nonlinear subfilter turbulence stress model for large-eddy simulation in the Advanced

Research WRF Model, Mon. Weather Rev., 138, 4212-4228, doi:10.1175/2010MWR3286.1.

Trabing, B. C., & Bell, M. M. (2021). The sensitivity of eyewall replacement cycles to shortwave radiation. Journal of Geophysical Research: Atmospheres, 126, e2020JD034016. https://doi. org/10.1029/2020JD034016

Wang, Y.-F., and Z.-M. Tan (2020), Outer Rainbands-Driven Secondary Eyewall Formation of Tropical Cyclones, J. Atmos. Sci., 6, 2217–2236, doi:10.1175/JAS-D-19-0304.1

Zhang, F., D. Tao, Y. Q. Sun, and J. D. Kepert (2017), Dynamics and predictability of secondary eyewall formation in sheared tropical cyclones, J. Adv. Model. Earth Syst., 9, 89–112, doi:10.1002/2016MS000729.

Zhu, Z., and P. Zhu (2014), The role of outer rainband convection in governing the eyewall replacement cycle in numerical simulations of tropical cyclones, J. Geophys. Res. Atmos., 119, 8049-8072, doi: 10.1002/2014JD021899.